frontiers in Materials

ORIGINAL RESEARCH
published: 24 June 2020
doi: 10.3389/fmats.2020.00197

Doubling the Mechanical Properties of Spider Silk by C_{60} Supersonic Molecular Beam Epitaxy

Maria F. Pantano[1], *Roberta Tatti*[2†], *Lucrezia Aversa*[2], *Roberto Verucchi*[2] *and Nicola M. Pugno*[1,3*]

[1] *Laboratory of Bio-Inspired, Bionic, Nano, Meta Materials and Mechanics, Department of Civil, Environmental and Mechanical Engineering, University of Trento, Trento, Italy,* [2] *Trento Unit C/O Fondazione Bruno Kessler, IMEM-CNR Institute of Materials for Electronics and Magnetism, Trento, Italy,* [3] *School of Engineering and Materials Science, Queen Mary University of London, London, United Kingdom*

OPEN ACCESS

Edited by:
Seunghwa Ryu,
Korea Advanced Institute of Science and Technology, South Korea

Reviewed by:
Dongchan Jang,
Korea Advanced Institute of Science and Technology, South Korea
Arun Nair,
University of Arkansas, United States

****Correspondence:***
Nicola M. Pugno
nicola.pugno@unitn.it

†Present address:
Roberta Tatti,
Laboratory of Biomarker Studies and Structure Analysis for Health, Fondazione Bruno Kessler, Trento, Italy

Specialty section:
This article was submitted to Mechanics of Materials, a section of the journal Frontiers in Materials

Received: *02 December 2019*
Accepted: *26 May 2020*
Published: *24 June 2020*

Citation:
Pantano MF, Tatti R, Aversa L, Verucchi R and Pugno NM (2020) Doubling the Mechanical Properties of Spider Silk by C_{60} Supersonic Molecular Beam Epitaxy. Front. Mater. 7:197. doi: 10.3389/fmats.2020.00197

Spider silk is one of the most fascinating natural materials, owing to its outstanding mechanical properties. In fact, it is able to combine usually self-excluding properties, like strength and toughness that synthetic fibers fail to replicate. Here, we report a method to further enhance the already excellent mechanical properties of spider's silk, producing nanocomposite fibers where the matrix of spider silk is reinforced with C_{60} molecules. These are deposited by Supersonic Molecular Beam Epitaxy (SuMBE) and are able to efficiently interact with silk, as evidenced by XPS analysis. As a consequence, upon proper adjustment of the fullerene kinetic energy, the treated fibers show improved strength, Young's modulus and toughness.

Keywords: spider silk, mechanical properties, fullerene, SuMBE, composites

INTRODUCTION

Spider silk is one of the most fascinating structural materials offered by nature owing to its unique capability of combining usually self-excluding properties, like load standing (e.g., strength) and energy dissipation (e.g., toughness). In particular, for long time spider's silk was believed to be the strongest among all natural materials (Vollrath, 2000) and only recently this was discovered to be surpassed by the limpet teeth (Barber et al., 2015).

The secret to spider silk's outstanding properties lies into the selection of its constituent macromolecules and their hierarchical supramolecular organization (Thiel et al., 1997), which has been the subject of intense studies that allowed mapping silk genetic sequence (Hayashi and Lewis, 2000). This provided useful information for the further improvement of spider silk properties or the development of novel bio-inspired materials. In fact, in order to overcome issues related to upscaling of spiders farming to a massive industrial level (Altman et al., 2003), transgenic silkworms were created encoding chimeric silkworm/spider silk genes able to produce composite fibers with improved mechanical properties (Teule et al., 2012). Another example was a recombinant protein that allowed mixing of the mechanical properties of spider silk with the capability of controlled nucleation and hydroxyapatite growth typical of dentin (Huang et al., 2007).

Unfortunately, the knowledge of the basic building blocks is not sufficient for a completely artificial yet efficient replication of silk fibers that would require also copying of the spider's spinning process. In fact, such process is characterized by significant complexity that is hard to be replicated by manufacturing tools currently available to humans (Vollrath and Knight, 2001). For this reason, there was a recent attempt to exploit spiders' spinning ability for production of composite silk fibers

reinforced with carbon nanotubes (CNTs) or graphene (Lepore et al., 2017). In that case, spiders after being exposed to CNT/graphene aqueous solutions were able to produce silk that resulted to contain those nanomaterials.

However, if spider silk cannot be fully reproduced artificially, it is possible to produce instead bio-inspired materials that take advantage of some of its features. For example, synthetic/natural ribbons and fibers with enhanced toughness were reported incorporating either dissipative structures in the form of slip knots (Pugno, 2014; Berardo et al., 2016; Bosia et al., 2016; Pantano et al., 2016) or looped metastructures (Koebley et al., 2017). Under application of a tensile load, loops unravel providing fibers/ribbons with an additional length (e.g., hidden length) that mimics the presence of sacrificial bonds in proteins structures (Fantner et al., 2006), thus allowing the possibility to accommodate large strain with consequent toughness improvement.

Apart from genetic engineering and bio-inspired design, spider silk can be exploited as raw material for production of functionalized composites by different techniques. For example, spider silk fibroin was blended with poly-DL-lactide (PDLLA) and electrospun in order to obtain biodegradable mats to be used for tissue engineering applications (Zhou et al., 2008). Alternatively, spider silk fibers were turn magnetic by superparamagnetic magnetite nanoparticles that covered their surfaces after immersion into colloidal sols (Mayes et al., 1998).

Here, we report on the design, fabrication and characterization of spider silk fibers reinforced with fullerenes (C_{60}). C_{60} molecules are well-characterized carbon allotropes, consisting of a cluster of 60 sp^2-bonded carbon atoms, which were shown to have interesting chemical and physical properties (Hedberg et al., 1991; Ruoff and Ruoff, 1991; Pawlak et al., 2011). Previous attempts of incorporation of fullerenes into other materials, such as aluminum (Tokunaga et al., 2008), proved their efficacy in improving the mechanical properties of the host matrix. However, different from other carbon allotropes, such as graphene or carbon nanotubes, its use as reinforcement material, especially in biological host matrices, such as spider silk, has been much less explored.

One of the common challenges to face when producing composites regards the homogeneous dispersion of the reinforcement materials. In this study, we do not use conventional mechanical methods, based on mixing and sonication. Instead, the composite fiber is prepared by depositing C_{60} onto silk fibers through an innovative approach for thin films deposition in Ultra High Vacuum (UHV) conditions, the Supersonic Molecular Beam Epitaxy (SuMBE). Such technique is based on the supersonic expansion in vacuum of a highly diluted gas mixture of a light gas carrier (usually noble gas), seeded by a heavier organic precursor. In case of fullerene, sublimation by thermal heating can be easily achieved and controlled, without introducing defects, degradation or decomposition. The C_{60} molecules, seeding the generating gas beam, experience an aerodynamic acceleration that, depending on the mass ratio between gas carrier and precursor, leads to a kinetic energy (KE) as high as several tens of eV and to a freezing of the molecular roto-vibrational modes. The large amount of translational kinetic energy reached by the precursor molecules in the beam can induce and activate chemical processes and surface diffusion. The possibility to control the thin film properties by changing the precursors kinetics in terms of beam source parameters, makes this approach particularly useful to (i) control the coalescence and diffusion process in the organic thin film growth (Wu et al., 2007; Nardi et al., 2010a); (ii) improve the crystallinity of inorganic material (Verucchi et al., 2012); (iii) synthesize carbon-based nanostructure (Verucchi et al., 2012; Tatti et al., 2016) and hybrid materials (Nardi et al., 2009; Tatti et al., 2017).

Studies conducted on C_{60} supersonic molecular beam have demonstrated that it is possible to break the fullerene cage at room temperature, during the collision of the organic molecule with the substrate, in order to synthesize a highly ordered silicon carbide. Exploiting the high KE of the C_{60} supersonic beam by SuMBE (about 30 eV), it was possible to synthesize high quality nanocrystalline 3C-SiC at room temperature using a C_{60} supersonic beam as precursor and Si(111) as substrate (Verucchi et al., 2012). Moreover, the SuMBE approach can give rise also to a strong chemical interaction between C_{60} and the Cu(111) substrate. The excess of energy, supplied by the C_{60} supersonic beam at a KE of 35 eV, induces a rearrangement of the C_{60} on the metal surface, promoting the fullerene cage breaking after thermal treatment and the formation of graphene flakes (Tatti et al., 2016).

In this work we show the possibility to extend these concepts also for the insertion of reinforcement nanoparticles in silk for the production of composite fibers with improved mechanical properties.

RESULTS AND DISCUSSION

In order to verify the beneficial effects that the addition of C_{60} molecules can play on the mechanical properties of spider silk, we took 18 samples from the dragline silk produced by the same spider that belongs to *Meta menardi* species. Three of these were used as control sample that provided reference values for the mechanical properties, while the remaining 15 specimens were divided in 5 groups and functionalized by C_{60} supersonic beams at different KE. In order to preserve the integrity of the C_{60} molecule during the deposition process, the C_{60} beam was used in a range of KE between 5 and 14 eV, and more specifically at 5, 8, 10, 12, and 14 eV. Particle arrival rate was kept constant for all depositions.

Silk specimens, fixed on a support to maintain fibers straight, were inserted in the analysis chamber, directly connected with the SuMBE apparatus, and decorated with a C_{60} film with an equivalent thickness of 5 monolayers (ML), as measured on a Cu surface used as reference (**Figure 1A**).

The mechanical behavior of the considered samples (**Figure 1B** shows an example spider silk fiber imaged by Scanning Electron Microscopy, SEM) was evaluated through tensile tests carried out on single fibers. **Figure 1C** reports one example curve for each sample type (see **Figure S1** for further details) while **Figure 2** collects the average values of strength, ultimate strain, Young's modulus and toughness for all tested samples. For the sake of comparison, these are reported as a function of SuMBE C_{60} KE. The histograms show that the deposition of C_{60} molecules has a significant influence on all

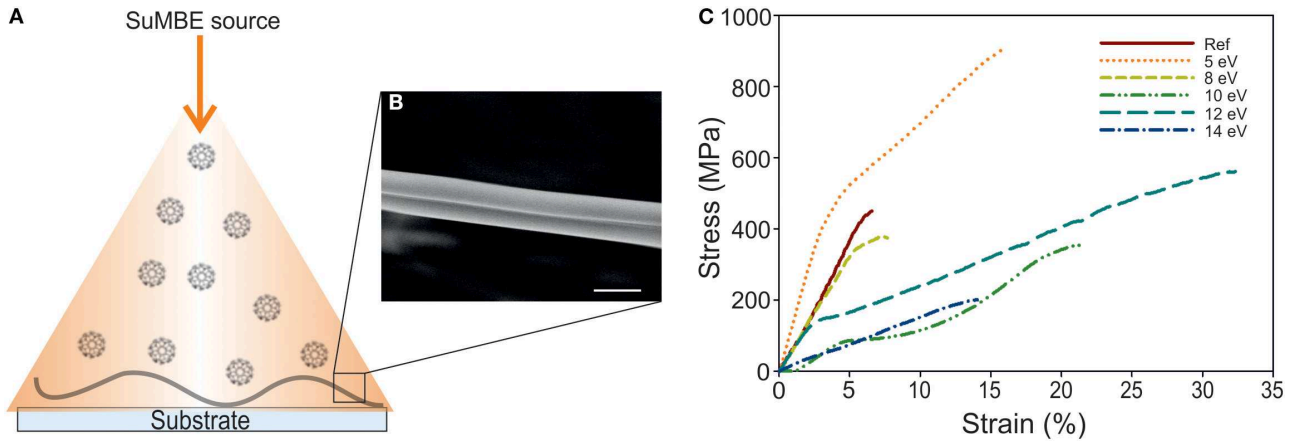

FIGURE 1 | (A) Schematic of the SuMBE process for C_{60} molecules deposition onto a spider silk fiber [detailed in the SEM image **(B)**. Scale bar: 2 μm]. During implantation, 5 ML of fullerenes were deposited. **(C)** Comparison between example stress-strain curves derived from tensile tests on raw fibers and SuMBE processed fibers at different KE (5, 8, 10, 12, and 14 eV). The example stress-strain curves here reported were selected as representative of their mean behavior and all are reported in the **Supplementary Material**.

the mechanical properties. Such effect can be clearly observed in spite of some data dispersion, which is not unexpected in the case of biological material samples, such as spider silk. Indeed, it is common to observe a certain variability across the stress-strain curves of spider silk fibers belonging to the same sample [as visible from the curves reported in **Figure S1A** or in other previous reports (Madurga et al., 2016)], which then causes variability in the values of the mechanical properties extracted from such curves.

With respect to reference, the smallest C_{60} KE (5 eV) corresponds to the highest increase possible of strength (1.7 times the reference value), Young's modulus (2.2 times the reference) and toughness (i.e., toughness modulus, defined as the area under the stress-strain curve; 2.7 times the reference); a significant increase of ultimate strain (1.6 times the reference) is also produced. Such simultaneous enhancement of the mechanical properties of our treated spider silk fibers is very interesting, in line with previous reports on the production of bio-inspired nanocomposite materials reinforced with carbon allotropes. For example, bionic spider silk incorporating carbon nanotubes showed an average increase in fracture strength, Young's modulus and toughness between 80 and 220%, while for bionic spider silk incorporating graphene the average increase was 15 and 60% (Lepore et al., 2017). For artificial nacre-like nanocomposites of copper and reduced graphene oxide, the addition of the graphene-based filler allowed an increase in the strength and Young's modulus of about 41% and 12%, respectively, with a toughness increase of up to 1.8 times (Xiong et al., 2015).

The strength increase observed in our treated silk fibers could be related to the increased number of hard crystal domains contained in the fibers after C_{60} deposition, which improves the already good load standing capability of the fibers, without however affecting their elongation capability. Such beneficial effect is however partially lost at higher KE levels, where probably the impinging supersonic beam causes some modification to the silk structure. This is particularly evident in the case of the highest KE that corresponds to the smallest values of both strength and ultimate strain, even if the reduction is not dramatic, especially in the case of strain (reduced by about 10%, while the strength is reduced to 1/3 of the reference vale). Thus, SuMBE treatment results not to compromise too much the silk structure, as it also emerges from imaging by SEM that does not reveal significant difference on the fibers after C_{60} implantation at different KE (**Figure S2**). Furthermore, it is interesting to notice that intermediate KEs of 10 and 12 eV have a slight negative effect on the strength, but beneficial effects in terms of ultimate strain that results to be 1.6 or 1.8 bigger than the reference value.

In order to clarify the chemical-physical process at the silk—C_{60} interface and evaluate the electronic properties of the bare silk after the deposition of C_{60}, X-ray photoelectron spectroscopy (XPS) analysis was performed on the two borderline cases: the silk "as it is" and after the deposition of 5 ML at the highest kinetic energy (14 eV). A cocoon produced by *Meta menardi* species, same spider used for the production of the dragline silk fibers, was used as reference silk sample. The cocoon was cut in half and mounted on a copper substrate, with the inner part exposed to the analysis and further C_{60} deposition (**Figure S3**).

The XPS characterization performed before and after the C_{60} SuMBE deposition reveals that the predominant elements in the silk are carbon, oxygen and nitrogen, leading also to a quantitative analysis of the chemical composition in terms of surface atomic percentage, as summarized in **Table 1**.

As expected, following the C_{60} deposition, the amount of carbon increases from 58.1 to 73.8%: 46.3% is related to the fullerene and the remaining 27.5 % is due to the silk. With reference to the latter component only, the evaluation of the silk related carbon content is highly influenced by the large fullerene signal, leading to its possible underestimation with lower C/N and C/O ratios, as indeed observed (see **Table 1**). Differently, the N/O ratio remains constant after C_{60} deposition suggesting that

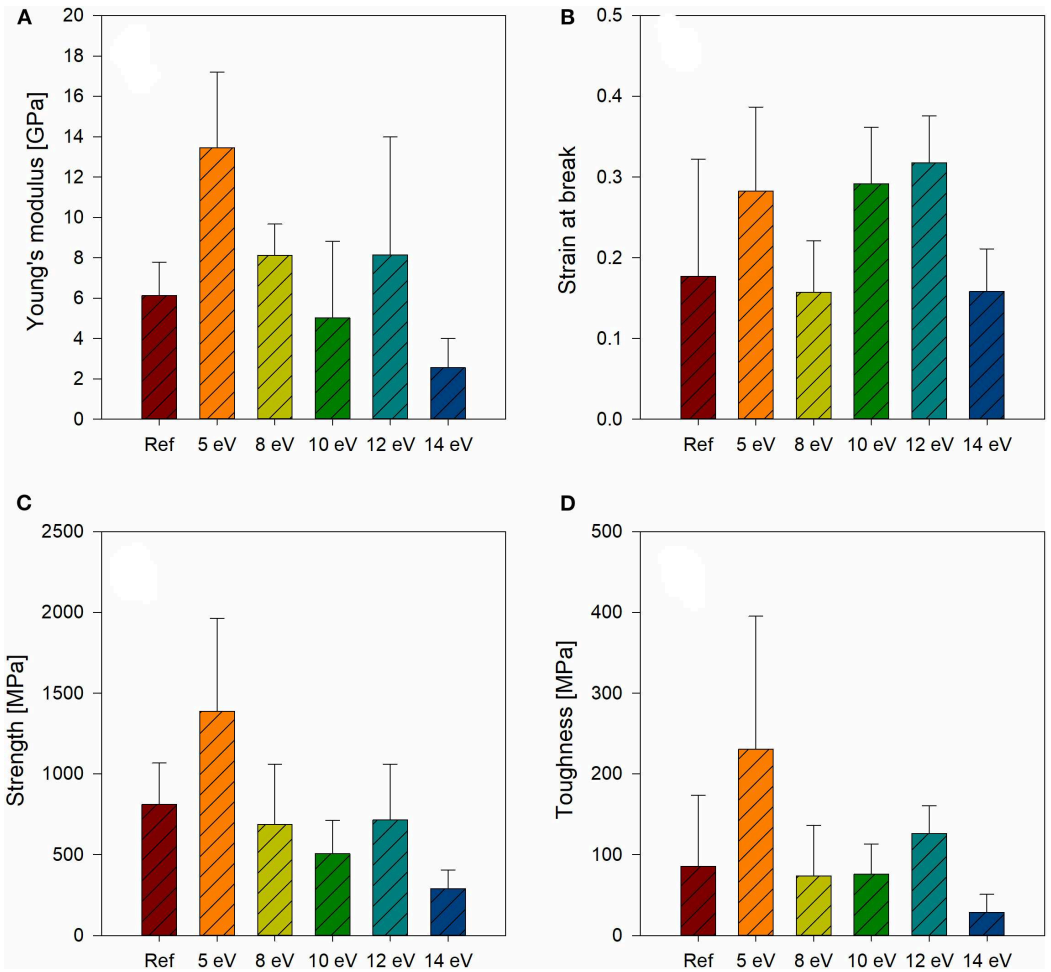

FIGURE 2 | Dependence of the Young's modulus **(A)**, strain at break **(B)**, strength **(C)** and, toughness **(D)** of spider silk fibers on the Kinetic Energy (KE) of Supersonic Molecular Beam Epitaxy (SuMBE) implantation of C_{60} molecules. A KE of 5 eV allows to almost double the Young's modulus, the strain at fracture and strength, while almost triple the toughness (here reported as the area under the stress-strain curve).

no contamination occurs during the SuMBE process. Thus, every eventual modification of the silk chemical/physical properties can be due only to the interaction with fullerene at 14 eV KE.

In order to get further insight about the interaction of silk and C_{60} molecules, we then investigated the lineshape and components of the C1s, O1s, and N1s core levels as shown in **Figure 3**. The features of all the components for the C1s, N1s, and O1s core levels, in terms of binding energy (BE), Full Width at Half Maximum (FWHM) and percentage calculated with respect to the total core level area, are summarized in **Table S1**. It is worth noting that all peaks show a shift toward higher binding energies, typically due to a charging effect related to the insulating character of these organic materials.

The C1s spectrum of the bare silk is characterized by four different components (see **Figure 3A**, upper panel), which reflect the chemical composition of the material. Indeed, silk is constituted by spidroin, a protein which is rich of glycine (Gly), alanine (Ala) and residues of other amino acids. This silk protein folds in a secondary structure characterized by crystalline regions, packed in β-sheets, interlocking with the adjacent chain via hydrogen bonds, and amorphous domains (**Figure 4**) (Hayashi et al., 1999; Hakimi et al., 2007).

TABLE 1 | Atomic percentage of all the chemical species present in the samples.

	C %	N %	O %	C*/N	C*/O	N/O
Spider Silk	59.7	22.8	17.5	2.6	3.4	1.3
C_{60} + Silk	73.8	15.4	10.8	1.8	2.6	1.4

Carbon considered in C/N and C/O ratios refers only to silk species. C only from silk.*

According to this description, the most intense component at 288.56 eV is related to carbon in the amide bond of the peptide chain, the latter being involved in hydrogen bonds between the oxygen and the nitrogen atom of the parallel amino acidic chains. As a matter of fact, the presence of the H bond increases the BE of the electronegative atoms (N, O), with the consequent decreasing of the carbon BE (Kerber et al., 1996; Garcia-Gil et al., 2013). The C-OH and amide groups not involved in hydrogen bonds,

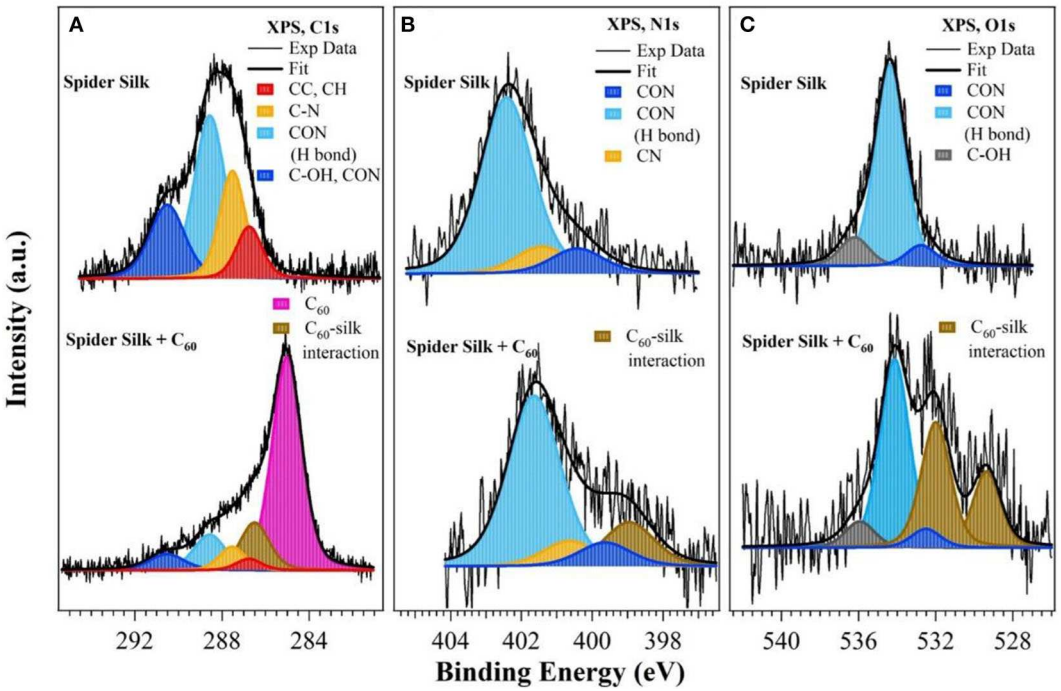

FIGURE 3 | Core level spectra (background subtracted): **(A)** C1s core level, **(B)** N1s core level and **(C)** O1s core level of the silk "as it is" and after the C_{60} deposition, from the top to the bottom, respectively.

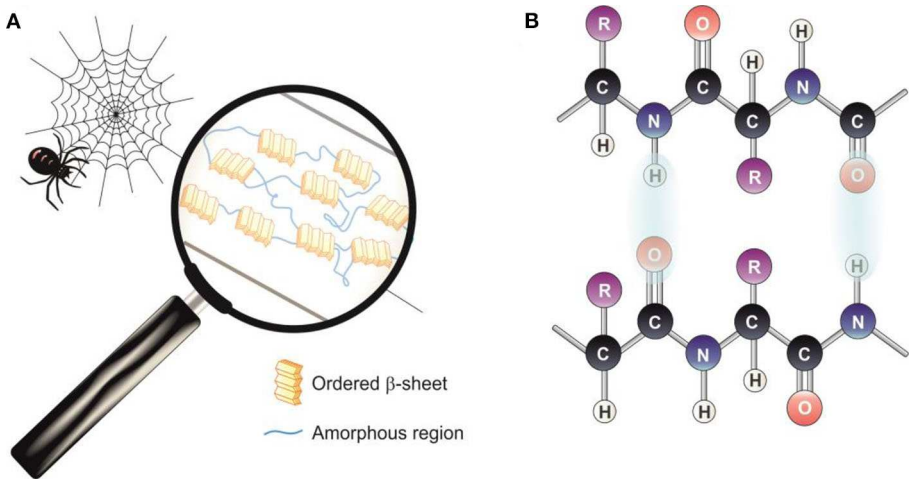

FIGURE 4 | (A) Schematic structure of spider silk. The yellow blocks are the highly ordered crystalline regions, joined by amorphous linkages. **(B)** Hydrogen bonds between parallel protein chains.

such as the substituents in the main chain and the components in the amorphous region, are located at higher BE (290.51 eV). The components at lower BE, 286.75 and 287.52 eV, are related, respectively, to the CC, CH, and CN groups of the substituents of the amino acids.

After the deposition of C_{60}, the deconvolution of the C1s core level lineshape is a superposition of the four features previously identified for silk, and the contribution stemming from the C_{60} (285.00 eV). Moreover, a new component is present at 286.50 eV (**Figure 3A**, bottom panel, brown color). It is not possible to exclude the presence of other peaks associated to this interaction overlapping the C_{60} signal, as indeed suggested by the large FWHM of this peak (1.6 eV), however their introduction would be merely a speculation, due to the complexity of the fitting and to the high number of species in the silk structure. What is worth is the presence of a new peak, suggesting this component belongs

to the interaction of silk chemical groups with the fullerene cages, and could justify the observed underestimation of silk carbon content (see **Table 1**).

The N1s core level of bare silk (**Figure 3B**, top panel) is constituted by a main component at higher BE (402.42 eV) related to the amidic group CON involved in hydrogen bond, a peak at 401.42 eV due to the CN groups of the substituents of the amino acids (Ariza et al., 2000), and a third component related to the CON groups not involved in hydrogen bonds, as observed for the C1s (**Figure 3B**, upper panel). The deposition of C_{60} on silk gives rise to a significant variation of the N1s lineshape (**Figure 3B**, bottom panel). The components related to silk shift by about −0.7 eV (401.64, 400.64, and 399.64 eV, respectively), and a new component is present at 398.95 eV (brown color). As for C1s lineshape analysis, this feature can be associated to the interaction of the C_{60} with the silk.

The O1s core level (**Figure 3C**, upper panel) of silk before the functionalization presents three features that can be related to the CON groups involved (534.38 eV) or not (532.76 eV) in hydrogen bonds, and the C-OH of the substituents (536.20 eV). After C_{60} deposition, these three contributions shift toward lower BE by about −0.3 eV. Moreover, two new peaks at lower BE (529.37 and 532.00 eV) are present, in agreement with what previously observed in C1s and N1s.

Being the N/O ratio constant in bare and C_{60} deposited silk, we can argue that all the new features observed in presence of C_{60} are related to silk chemical groups that suffered a significant modification with respect to the pristine material, while the presence of fingerprints of the original silk structure for all elements suggests modifications are related to specific protein sites. Concerning N1s and O1s analysis, the appearance of new peaks at lower BE suggests breaking of H bonds between CO and N-H, probably due to impingement of the C_{60} cage at 14 eV, a process leading to reduction of silk mechanical properties. Due to the low concentration of nitrogen and oxygen, such an effect cannot be identified in C1s peak analysis. Conversely, the new intense peak at 286.5 eV, very close to the C_{60} main one, could be due to formation of chemical bonds between fullerene and silk chains thanks to the molecule high electronegativity, e.g., promoting link with amide group (López et al., 2011; Umeyama and Imahori, 2013). The balance between the two processes probably determines the increase or decrease of mechanical properties at the different C_{60} KEs.

CONCLUSIONS

In conclusion, we have shown an alternative method for producing spider silk composite fibers with improved mechanical properties requiring no genetic engineering. Raw spider silk fibers were in fact reinforced with C_{60} molecules via a high energy well assessed technique, like SuMBE. Upon optimization of the process parameters, thus of the fullerene translational KE, it is possible to obtain an almost 2-fold increase of strength and an almost 3-fold increase of toughness. Such method could be used in future also for fabrication of other high-performance nanocomposites considering different fibers as matrix.

A cocoon of spider silk was analyzed *ex situ* by XPS, before and after functionalization with C_{60} at high KE (14 eV). The analysis demonstrated the presence of fullerenes in silk, and the formation of new chemical species between silk and C_{60}, confirming the efficiency of the SuMBE approach for the functionalization of spider silk. Moreover, the deep analysis of the C1s, O1s, and N1s core levels put in evidence that the C_{60} deposition reflects in a structural modification of the silk itself. Indeed, new components are present in all the analyzed core levels, suggesting that this interaction affects the whole silk structure and constituents.

It is difficult to interpret the origin of the new components appearing after the deposition. Their intensity and presence in all silk elemental constituents suggest a strong and diffused functionalization, involving all groups and related connections. The mechanical properties show a modification of the silk structure, an evidence that can be interpreted, from a chemical point of view, as the rupture of specific chemical bonds, as well as the formation of other bonds with C_{60} molecules. The interplay of these two effects (the breaking and formation of new species/bonds) is guided by the C_{60} KE as well as by the number of deposited molecules and leads to the observed silk changed mechanical properties. Further experiments will be devoted to study in details the interplay between all parameters.

MATERIALS AND METHODS

Film Deposition and Analysis Apparatus

The deposition of C_{60} and the characterization by X-ray photoelectron spectroscopy of only the spider cocoon, were performed using an experimental setup devoted to the thin film growth and *in-situ* analysis in UHV conditions.

The SuMBE apparatus consists of two chambers at different stages of vacuum (10^{-4} and 10^{-7} mbar, respectively). The supersonic source is located in the first chamber (source chamber) and it is essentially made of a quartz tube (12 cm length) with a nozzle (50 μm of diameter) at the front closed end, whereas in the back end the carrier gas is injected (Helium). The source is resistively heated by a Ta foil, which can reach a maximum temperature of about 1,000°C. The second chamber, instead, acts as an interface between the beam chamber and the final UHV deposition chamber, working as a differential pumping stage. The beam geometry and axis is defined by two collimators (skimmers), one positioned between the first and the second chamber on the axis of the vacuum system, and the other one between the second chamber and the analysis chamber. The first skimmer allows to extract the supersonic "molecular" beam out of the zone of silence of the supersonic expansion, working as a diaphragm between the two vacuum chambers. The second skimmer, maintains a differential vacuum between the second chamber and the analysis chamber and defines the size of the beam spot downstream of the generation apparatus (Nardi et al., 2010b).

The kinetic energy of the fullerene beam is tuned changing the pressure of the buffered gas and the source temperature to which the fullerene is evaporated, ranging from 5 to 14 eV. The

typical organic arrival rate on the substrate was about 1Å/min, as evaluated from a quartz microbalance, and was kept constant during all the experiments. A film of about 5 ML was deposited on the material, with a nominal thickness of about 4 nm. The C_{60} material was supplied by Sigma Aldrich, with a nominal purity of 99.9%.

The source chamber is directly connected by a valve to a μ-metal chamber (pressure $7x10^{-11}$ mbar), where the film deposited on the silk cocoon can be characterized by XPS *in situ*, avoiding air contamination. XPS is performed using the Mg-Kα emission at 1253.6 eV as X-ray photon source. The photoelectrons are analyzed by a VSW HA100 electron energy analyzer, leading to a total energy resolution of 0.86 eV. Core level BEs are referred to the Au 4f7/2 core level signal (at 84.0 eV), obtained from a sputtered gold surface. The photoemission core levels of all elements are analyzed through Voight lineshape deconvolution, after background subtraction of a Shirley function. The typical precision for energy peak position is ±0.05 eV, while uncertainty for FWHM is $< \pm 5\%$ and for area evaluation it is ±5%.

Mechanical Characterization

Tensile tests on single spider silk fibers were carried out through the Nanotensile Tester UTM150 by Agilent at room temperature and at a strain rate of 0.001 s^{-1}. Tested fibers length was about 10 mm.

DATA AVAILABILITY STATEMENT

All datasets generated for this study are included in the article/**Supplementary Material**.

AUTHOR CONTRIBUTIONS

NP designed and coordinated the study. MP analyzed the data from the mechanical tests. RT, LA, and RV performed SuMBE and XPS analysis. All the authors discussed the results and approved the manuscript.

ACKNOWLEDGMENTS

The authors thank E. Lepore for the help in the mechanical characterization. NP is supported by the European Commission under the FET Proactive (Neurofibres) grant no. 732344, as well as by the Italian Ministry of Education, University and Research (MIUR) under the ARS01-01384-PROSCAN and the PRIN-20177TTP3S grants.

SUPPLEMENTARY MATERIAL

The Supplementary Material for this article can be found online at: https://www.frontiersin.org/articles/10.3389/fmats.2020.00197/full#supplementary-material

REFERENCES

Altman, G. H., Diaz, F., Jakuba, C., Calabro, T., Horan, R. L., Chen, J., et al. (2003). Silk-based biomaterials. *Biomaterials* 24, 401–416. doi: 10.1016/S0142-9612(02)00353-8

Ariza, M. J., Rodriguez-Castellon, E., Rico, R., Benavente, J., Munoz, M., and Oleinikova, M. (2000). X-Ray photoelectron spectroscopy analysis of Di-(2-ethylhexyl) phosphoric acid activated membranes. *J. Colloid Interface Sci.* 226, 151–158. doi: 10.1006/jcis.2000.6805

Barber, A. H., Lu, D., and Pugno, N. (2015). Extreme strength observed in limpet teeth. *J. Roy. Soc. Interf.* 12:1326. doi: 10.1098/rsif.2014.1326

Berardo, A., Pantano, M. F., and Pugno, N. (2016). Slip knots and unfastening topologies enhance toughness without reducing strength of silk fibroin fibres. *Interf. Focus* 6:60. doi: 10.1098/rsfs.2015.0060

Bosia, F., Lepore, E., Alvarez, N. T., Miller, P., Shanov, V., and Pugno, N. (2016). Knotted synthetic polymer or carbon nanotube microfibres with enhanced toughness, up to 1400 J/g. *Carbon* 102, 116–125. doi: 10.1016/j.carbon.2016.02.025

Fantner, G. E., Oroudjev, E., Schitter, G., Golde, L. S., Thurner, P., Finch, M. M., et al. (2006). Sacrificial bonds and hidden length: unraveling molecular mesostructures in tough materials. *Biophys. J.* 90, 1411–1418. doi: 10.1529/biophysj.105.069344

Garcia-Gil, S., Arnau, A., and Garcia-Lekue, A. (2013). Exploring large O 1s and N 1s core level shifts due to intermolecular hydrogen bond formation in organic molecules. *Surf. Sci.* 613, 102–107. doi: 10.1016/j.susc.2013.03.017

Hakimi, O., Knight, D. P., Vollrath, F., and Vadgama, P. (2007). Spider and mulberry silkworm silks as compatible biomaterials. *Composites* 38, 324–337. doi: 10.1016/j.compositesb.2006.06.012

Hayashi, C. Y., and Lewis, R. V. (2000). Molecular architecture and evolution of a modular spider silk protein gene. *Science* 287, 1477–1479. doi: 10.1126/science.287.5457.1477

Hayashi, C. Y., Shipley, N. H., and Lewis, R. V. (1999). Hypotheses that correlate the sequence, structure, and mechanical properties of spider silk proteins. *Int. J. Biol. Macromol.* 24, 271–275. doi: 10.1016/S0141-8130(98)00089-0

Hedberg, K., Hedberg, L., Bethune, D. S., Brown, C. A., Dorn, H. C., Johnson, R. D., et al. (1991). Bond lengths in free molecules of buckminsterfullerene, C_{60}, from gas-phase electron diffraction. *Science* 254, 410–412. doi: 10.1126/science.254.5030.410

Huang, J., Wong, C., George, A., and Kaplan, D. L. (2007). The effect of genetically engineered spider silk-dentin matrix protein 1 chimeric protein on hydroxyapatite nucleation. *Biomaterials* 28, 2358–2367. doi: 10.1016/j.biomaterials.2006.11.021

Kerber, S. J., Bruckner, J. J., Wozniak, K., Seal, S., Hardcastle, S., and Barr, T. L. (1996). The nature of hydrogen in x-ray photoelectron spectroscopy: general patterns from hydroxides to hydrogen bonding. *J. Vacuum Sci. Technol.* 14:1314. doi: 10.1116/1.579947

Koebley, S. R., Vollrath, F., and Schniepp, H. C. (2017). Toughness-enhancing metastructure in the recluse spider's looped ribbon silk. *Mat. Horiz.* 4, 377–382. doi: 10.1039/C6MH00473C

Lepore, E., Bonaccorso, F., Bruna, M., Bosia, F., Taioli, S., Garberoglio, G., Ferrari, A. C., and Pugno, N. M. (2017). Silk reinforced with graphene or carbon nanotubes spun by spiders. *2D Materials* 4:031013. doi: 10.1088/2053-1583/aa7cd3

López, A. M., Mateo-Alonso, A., and Prato, M. (2011). Materials chemistry of fullerene C60 derivatives. *J. Mater. Chem.* 21, 1305–1318. doi: 10.1039/C0JM02386H

Madurga, R., Plaza, G. R., Blackledge, T. A., Guinea, G. V., Elices, M., and Perez-Rigueiro, J. (2016). Material properties of evolutionary diverse spider silks described by variation in a single structural parameter. *Sci. Rep.* 6:18991. doi: 10.1038/srep18991

Mayes, E. L., Vollrath, F., and Mann, S. (1998). Fabrication of magnetic spider silk and other silk-fiber composites using inorganic nanoparticles. *Adv. Mater.* 10, 801–805.

Nardi, M., Verucchi, R., Aversa, L., Casarin, M., Vittadini, A., Mahne, N., et al. (2010a). Electronic properties of tetrakis(pentafluorophenyl)porphyrin. *New J. Chem.* 37:1036. doi: 10.1039/c3nj40910d

Nardi, M., Verucchi, R., Corradi, C., Pola, M., Casarin, M., Vittadini, A., et al. (2010b). Tetraphenylporphyrin electronic properties: a combined theoretical

and experimental study of thin films deposited by SuMBD. *Phys. Chem. Chem. Phys.* 12, 871–880. doi: 10.1039/B914847G

Nardi, M., Verucchi, R., Tubino, R., and Iannotta, S. (2009). Activation and control of organolanthanide synthesis by supersonic molecular beams: erbium-porphyrin test case. *Phys. Rev. B* 79:125404. doi: 10.1103/PhysRevB.79.125404

Pantano, M. F., Berardo, A., and Pugno, N. (2016). Tightening slip knots in raw and degummed silk to increase toughness without losing strength. *Sci. Rep* 6:18222. doi: 10.1038/srep18222

Pawlak, R., Kawai, S., Fremy, S., Glatzel, T., and Meyer, E. (2011). Atomic-scale mechanical properties of orientated C_{60} molecules revealed by noncontact atomic force microscopy. *ACS Nano* 5, 6349–6354. doi: 10.1021/nn201462g

Pugno, N. (2014). The "Egg of Columbus" for making the world's toughest fibres. *PLoS ONE* 9:e93079. doi: 10.1371/journal.pone.0093079

Ruoff, R. S., and Ruoff, A. L. (1991). Is C_{60} stiffer than diamond? *Nature* 350, 663–664. doi: 10.1038/350663b0

Tatti, R., Aversa, L., Verucchi, R., Cavaliere, E., Garberoglio, G., Pugno, N. M., et al. (2016). Synthesis of single layer graphene on Cu(111) by C_{60} supersonic molecular beam epitaxy. *RSC Adv.* 6:37982. doi: 10.1039/C6RA02274J

Tatti, R., Timpel, M., Nardi, M. V., Fabbri, F., Rossi, R. L., Pasquardini, A., et al. (2017). Functionalization of SiC/SiOx nanowires with a porphyrin derivative: a hybrid nanosystem for X-ray induced singlet oxygen generation. *Mol. Syst. Des. Eng.* 2, 165–172. doi: 10.1039/C7ME00005G

Teule, F., Miao, Y.-G., Sohn, B.-H., Kim, Y.-S., Hulla, J. J., Fraser, M. J. Jr., Lewis, R. V., and Jarvis, D. L. (2012). Silkworms transformed with chimeric silkworm/spider silk genes spin composite silk fibers with improved mechanical properties. *Proc. Natl. Acad. Sci. U.S.A.* 109, 923–928. doi: 10.1073/pnas.1109420109

Thiel, B. L., Guess, K. B., and Viney, C. (1997). Non-periodic lattice crystals in the hierarchical microstructure of spider (major ampullate) silk. *Biopolymers* 41, 703–719.

Tokunaga, T., Kaneko, K., Sato, K., and Horita, Z. (2008). Microstructure and mechanical properties of aluminum–fullerene composite fabricated by high pressure torsion. *Scr. Mater.* 58, 735–738. doi: 10.1016/j.scriptamat.2007.12.010

Umeyama, T., and Imahori, H. (2013). Photofunctional hybrid nanocarbon materials. *J. Phys. Chem. C* 117, 3195–3209. doi: 10.1021/jp309149s

Verucchi, R., Aversa, L., Nardi, M. V., Taioli, S., Beccara, S. A., Alfˌè, D., et al. (2012). Iannotta, epitaxy of nanocrystalline silicon carbide on Si(111) at room temperature. *J. Am. Chem. Soc.* 134:17400. doi: 10.1021/ja307804v

Vollrath, F. (2000). Strength and structure of spiders' silks. *Rev. Mol. Biotechnol.* 74, 67–83. doi: 10.1016/S1389-0352(00)00006-4

Vollrath, F., and Knight, D. P. (2001). Liquid crystalline spinning of spider silk. *Nature* 410, 541–548. doi: 10.1038/35069000

Wu, Y., Toccoli, T., Koch, N., Iacob, E., Pallaoro, A., Rudolf, P., and Iannotta, S. (2007). Controlling the early stages of pentacene growth by supersonic molecular beam deposition. *Phys. Rev. Lett.* 98:076601. doi: 10.1103/PhysRevLett.98.076601

Xiong, D.-B., Cao, M., Guo, Q., Tan, Z., Fan, G., Li, Z., et al. (2015). Graphene-and-copper artificial nacre fabricated by a preform impregnation process: bioinspired strategy for strengthening-toughening of metal matrix composite. *ACS Nano* 9, 6934–6943. doi: 10.1021/acsnano.5b01067

Zhou, S., Peng, H., Yu, X., Zheng, X., Cui, W., Zhang, Z., et al. (2008). Preparation and characterization of a novel electrospun spider silk fibroin/Poly(D,L-lactide) composite fiber. *J. Phys. Chem. B* 112, 11209–11216. doi: 10.1021/jp800913k

Conflict of Interest: The authors declare that the research was conducted in the absence of any commercial or financial relationships that could be construed as a potential conflict of interest.

Supporting Information

Doubling the Mechanical Properties of Spider Silk by C_{60} Supersonic Molecular Beam Epitaxy

Maria F. Pantano[1], Roberta Tatti[2]†, Lucrezia Aversa[2], Roberto Verucchi[2], Nicola M. Pugno[1,3*]

[1]Laboratory of Bio-Inspired, Bionic, Nano, Meta Materials & Mechanics, Department of Civil, Environmental and Mechanical Engineering, University of Trento, 38123 Trento, Italy

[2]IMEM-CNR Institute of Materials for Electronics and Magnetism, Trento unit c/o Fondazione Bruno Kessler, Via alla Cascata 56/C, Povo – 38123 Trento (Italy)

[3] School of Engineering and Materials Science, Queen Mary University of London, Mile End Road, E1 4NS London, United Kingdom

†current address: Laboratory of Biomarker Studies and Structure Analysis for Health, Fondazione Bruno Kessler, Via Sommarive 18, 38123, Trento, Italy

**Corresponding author: nicola.pugno@unitn.it*

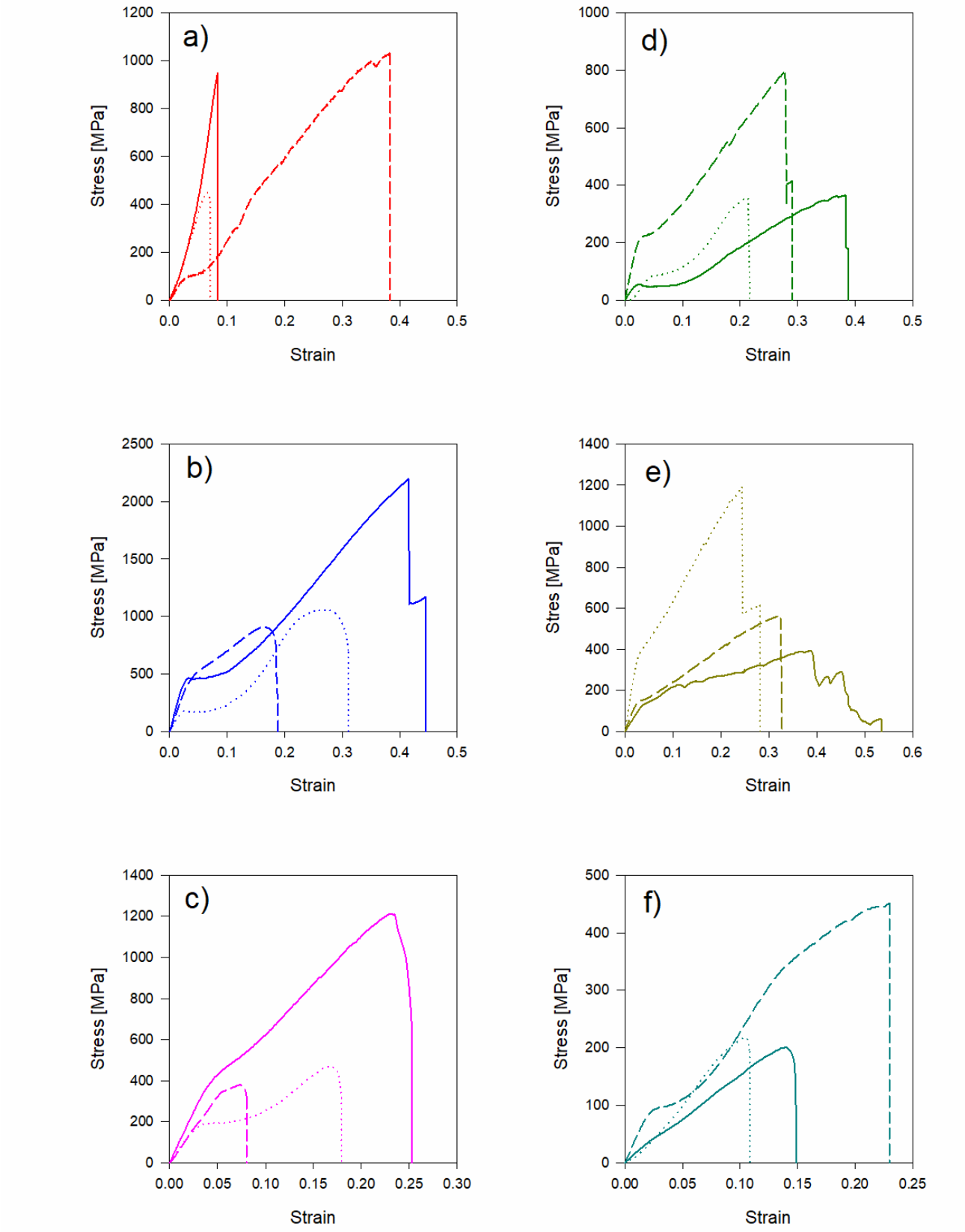

Figure S1: Stress strain curves of (a) as-produced and spider silk fibers treated with a C_{60} supersonic beam at C_{60} kinetic energy of 5 (b), 8 (c), 10 (d), 12 (e), 14 (f) eV.

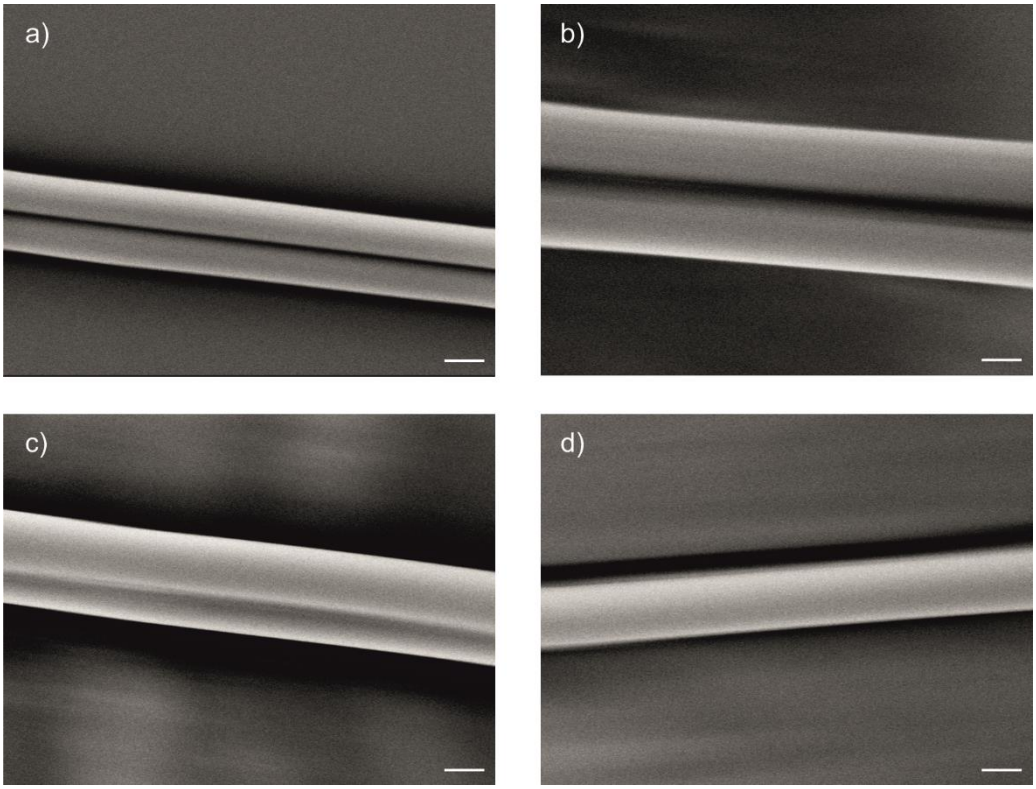

Figure S2: SEM images of spider silk fibers treated after C_{60} SuMBE at 8 (a), 10 (b), 12 (c), 14 (d) eV. No evidence of damage can be observed. Scale bar: 1 µm.

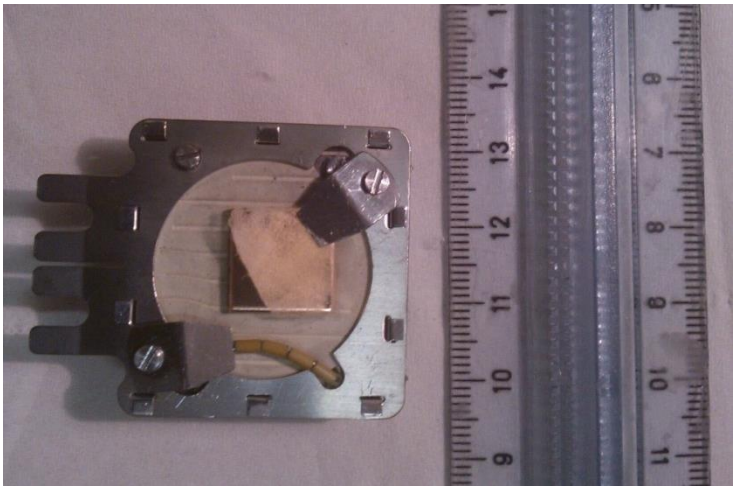

Figure S3: Sample of a spider cocoon mounted on a copper substrate for the XPS analysis.

Table S1. Main components of C1s, N1s and O1s core levels for the silk “as it is” and after the deposition of 5 ML of C_{60}.

		Spider Silk			Spider Silk + C_{60}		
		BE [eV]	**FWHM [eV]**	**%**	**BE [eV]**	**FWHM [eV]**	**%**
C1s	CC, CH	286.75	1.4	11.4	286.76	1.4	2.9
	CN	287.52	1.4	23.5	287.52	1.4	5.9
	CON main chain (H bond)	288.56	1.7	43.2	288.57	1.7	10.9
	COH, CON substituents	290.51	1.9	21.9	290.52	1.9	5.5
	C_{60}				285.01	1.6	61.1
	Interaction Silk-C_{60}				286.50	1.6	13.7
N1s	CON substituents	400.42	1.75	11.1	399.64	1.75	9.1
	CN	401.42	1.75	11.9	400.64	1.75	9.7
	CON main chain (H bond)	402.42	1.75	77.0	401.64	1.75	64.9
	Interaction Silk-C_{60}				398.95	1.70	16.33
O1s	CON substituents	532.76	1.8	8.3	532.51	1.8	4.4
	CON main chain (H bond)	534.38	1.8	80.2	534.13	1.8	43.7
	COH	536.20	1.8	11.5	535.93	1.8	6.1
	Interaction Silk-C_{60}				529.37	1.7	16.7
					532.00	1.8	29.1